Output current ripple analysis of single phase inverter with discontinuous PWM

Anwar Muqorobin[1], Sulistyo Wijanarko[1], Harjono Priyo Santosa[1], Indrarini Dyah Irawati[2]
[1]Research Center for Energy Conversion and Conservation, National Research and Innovation Agency, Bandung, Indonesia
[2]School of Applied Science, Telkom University, Bandung, Indonesia

Article Info

Article history:

Received Sep 29, 2023
Revised May 2, 2024
Accepted May 22, 2024

Keywords:

DPWM
Modulation index
Output current ripple
Single phase inverter
SPWM

ABSTRACT

Voltage source inverter has been applied for uninterruptible power supply (UPS), renewable energy sources, and motor drive. The popular modulations for inverters are sinusoidal pulse width modulation (SPWM), zero sequence signal modulation (ZSS), space vector modulation (SVM), and discontinuous PWM (DPWM). All these modulations have been applied to three-phase and multiphase inverters. The characteristics of the modulation application in these inverters have been well investigated. However, only SPWM has been applied satisfactorily in single-phase inverter. From the literature, the applications of ZSS and DPWM couldn't show any benefit. In this paper, a DPWM is proposed for single-phase inverter. The output current ripple is analyzed and experiments are conducted to verify the analytical result. Comparison to SPWM is conducted to find the modulation index range that provides a benefit when using the DPWM.

Corresponding Author:

Anwar Muqorobin
Research Center for Energy Conversion and Conservation, National Research and Innovation Agency
KST Samaun Samadikun, Bandung, Indonesia
Email: anwa014@brin.go.id

1. INTRODUCTION

Single-phase inverters have been applied in motor drives, UPS, and renewable energy sources [1]-[7]. Much literature has been published related to single-phase inverter. Among them can be categorized into inverter topology, control algorithm, and modulation technique [4]-[13]. Many inverter topologies have been proposed e.g. half/full bridge inverter, multilevel inverter, H5/H6 inverter, T-type inverter, HERIC inverter, and differential inverter [4]-[6], [12]-[15]. Single-phase full bridge inverter gives high efficiency and high-reliability characteristics. However, it needs a large DC link capacitor to absorb the ripples through it i.e. high frequency voltage/current ripple and low frequency 2ω ripple.

The SPWM for a single-phase full bridge inverter can be divided into bipolar and unipolar modulations. A single-phase full-bridge inverter has two legs of switching components. In bipolar modulation, one reference is used for the two legs. The two legs get opposite commands. Unipolar modulation uses two references that are 180º out of phase for both legs. This modulation can be divided into two types i.e. asymmetrical and symmetrical modulations. Asymmetrical modulation allows one leg to be switched with high frequency and the other leg to be switched with fundamental frequency. Thus, the losses in the two legs are not balanced. Whereas in symmetrical modulation, both legs are switched at the same frequency. Symmetrical unipolar modulation provides the smallest output current ripple compared to asymmetrical unipolar and bipolar modulations [16].

Besides SPWM, other types of modulations that can be found in the literature are ZSS, SVM, and DPWM. These modulation types have been applied successfully in three-phase and multiphase inverters

[17]-[24]. However, the successful application in single-phase inverters is still rarely reported in literature. The application of ZSS in a single-phase inverter cannot increase the linear modulation range [25]. Several DPWMs also have been proposed [25]-[29]. However, the proposed DPWMs in [27], [28] produce low-order harmonics. In this paper, a DPWM is proposed which has the advantage of being simple and does not produce low-order harmonics. The output current ripple is derived and experimental results are also presented. The output current ripple of the DPWM is compared to SPWM to find out the modulation index range which can provide an advantage when using DPWM.

2. RESEARCH METHOD

2.1. Output current ripple analysis

The single-phase full bridge inverter is shown in Figure 1(a). A single-phase full-bridge inverter converts a DC voltage to an AC voltage by using a modulation technique to the bridge circuit. The bridge circuit is made of semiconductor switching devices e.g. MOSFET or IGBT. Then, a filter is used to produce sinusoidal current and voltage. The reference signals of the proposed DPWM for legs A and B are shown in Figure 1(b). As we can see, the waveform pattern is repeated every $\pi/2$ interval. The equations of the reference signals are shown in Table 1. These reference signals are sinusoidal signals with signal injection as shown in the table. At the angle values less than gamma (we call here a discontinuous angle), sinusoidal references are used. At the angle values above gamma, a discontinuous reference is introduced.

The reference signal is compared to a carrier signal to produce the ON-OFF signal for the inverter leg. If the reference signal is higher than the carrier signal, an ON signal is produced. This means the upper switching component is switched and the lower switching component is left to be open. The OFF signal is produced when the reference signal is lower than the carrier signal. In this situation, it is the lower switching component that is to be switched and the upper switching device is left to be open. The waveforms during a switching period T_s are shown in Figures 2(a) and 2(b), each for angles less than gamma and more than gamma, respectively.

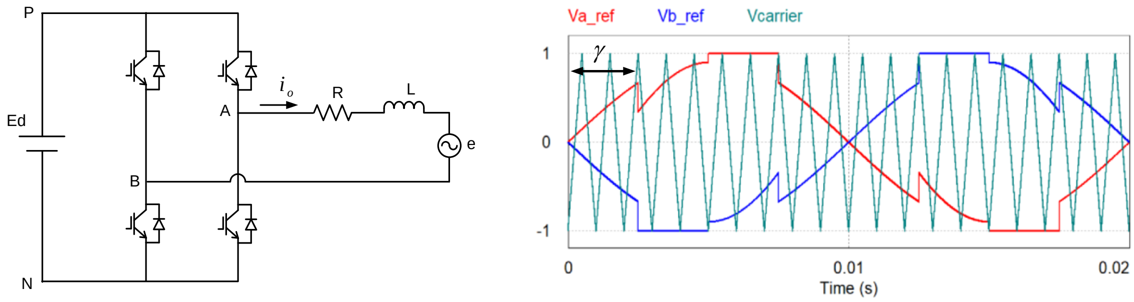

(a) (b)

Figure 1. Single phase full bridge inverter: (a) circuit and (b) DPWM reference signals

Table 1. DPWM reference signals

Interval	Signal Injection	v_A^r	v_B^r
$0 \le \theta < \gamma$	0	$k\sin(\theta)$	$-k\sin(\theta)$
$\gamma \le \theta < \pi/2$	$-1 + k\sin(\theta)$	$2k\sin(\theta) - 1$	-1
$\pi/2 \le \theta < \pi - \gamma$	$1 - k\sin(\theta)$	1	$1 - 2k\sin(\theta)$
$\pi - \gamma \le \theta < \pi$	0	$k\sin(\theta)$	$-k\sin(\theta)$
$\pi \le \theta < \pi + \gamma$	0	$k\sin(\theta)$	$-k\sin(\theta)$
$\pi + \gamma \le \theta < 3\pi/2$	$1 + k\sin(\theta)$	$2k\sin(\theta) + 1$	1
$3\pi/2 \le \theta < 2\pi - \gamma$	$-1 - k\sin(\theta)$	-1	$-1 - 2k\sin(\theta)$
$2\pi - \gamma \le \theta < 2\pi$	0	$k\sin(\theta)$	$-k\sin(\theta)$

To analyze the output current ripple, firstly the mean square value of the current ripple during the switching period is formulated. After that, the mean square value during a fundamental period is calculated. The switching period is determined by the frequency of the carrier signal and the fundamental period by the reference signal. The carrier frequency is much higher than the reference signals. As a result, the reference signals are assumed to be constant during the switching period.

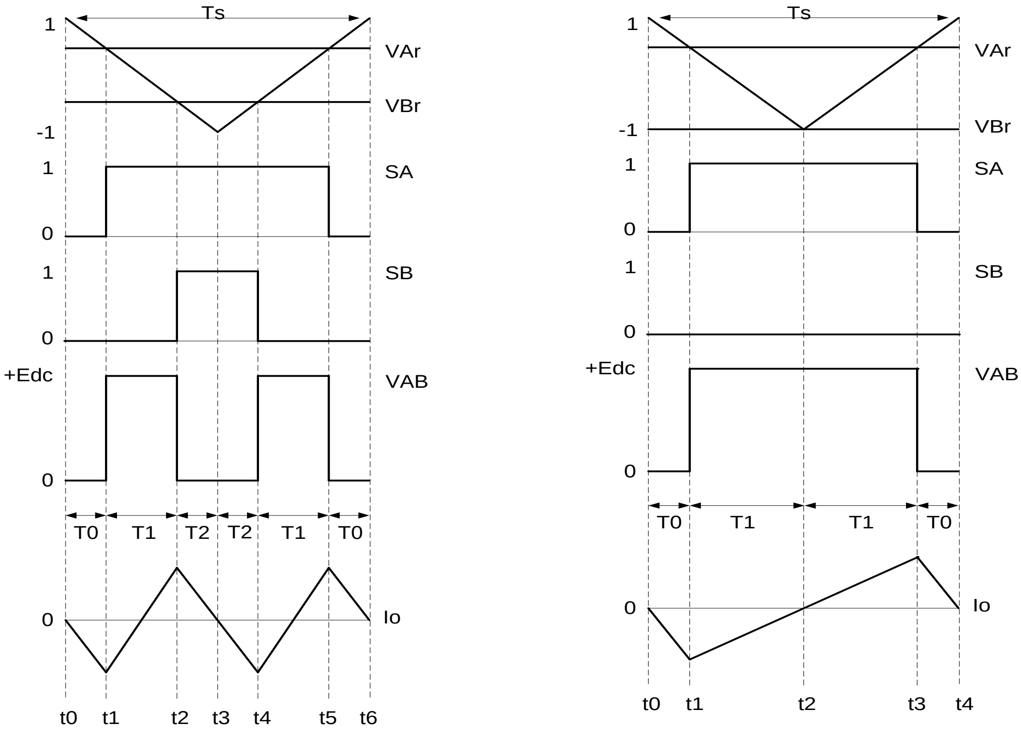

(a) (b)

Figure 2. The waveforms during a switching period (a) interval of $0 \leq \theta < \gamma$ and (b) interval of $\gamma \leq \theta < \pi/2$

From Figure 1(a), the inverter output voltage can be represented as (1).

$$v_{AB} = Ri_o + L\frac{di_o}{dt} + e \quad (1)$$

Because of the switching action, the voltage and the current consist of their average and the ripple components. The (1) can be written as (2).

$$\bar{v}_{AB} + \tilde{v}_{AB} = R(\bar{i}_o + \tilde{i}_o) + L\frac{d(\bar{i}_o+\tilde{i}_o)}{dt} + e \quad (2)$$

The above equation can be separated into the average (3) and the ripple (4), i.e.

$$\bar{v}_{AB} = R\bar{i}_o + L\frac{d\bar{i}_o}{dt} + e \quad (3)$$

$$\tilde{v}_{AB} = R\tilde{i}_o + L\frac{d\tilde{i}_o}{dt} \quad (4)$$

The ripple voltage drop across the resistance R is much smaller than the one across the inductor. So, from (4) the expression for the output current ripple can be represented as (5).

$$\tilde{i}_o \approx \frac{1}{L}\int(v_{AB} - \bar{v}_{AB})dt \quad (5)$$

The average value of the output voltage is in (6).

$$\bar{v}_{AB} = E_d k \sin(\theta) \quad (6)$$

In (1) to (6) v_{AB} is the voltage between points A and B, R is the load resistance, L is the load inductance, i_o is the output current, e is the back electromotive force, $\bar{\cdot}$ is the average value, $\tilde{\cdot}$ is the ripple value, E_d is the DC input voltage, k is the modulation index, $\theta = 2\pi f_o t$ is the angle, f_o is the fundamental frequency, and t is the time.

Based on Figure 2(a), the current ripple in the interval of $0 \leq \theta < \gamma$ can be represented as (7).

$$\tilde{\imath}_{o1} = \begin{cases} \left(\frac{-\bar{v}_{AB}}{L}\right)(t-t_0) & , \quad t_0 \le t \le t_1 \\ \left(\frac{E_d-\bar{v}_{AB}}{L}\right)(t-t_1) + \left(\frac{-\bar{v}_{AB}}{L}\right)T_0 & , \quad t_1 \le t \le t_2 \\ \left(\frac{-\bar{v}_{AB}}{L}\right)(t-t_3) & , \quad t_2 \le t \le t_4 \\ \left(\frac{E_d-\bar{v}_{AB}}{L}\right)(t-t_4) + \left(\frac{-\bar{v}_{AB}}{L}\right)T_2 & , \quad t_4 \le t \le t_5 \\ \left(\frac{-\bar{v}_{AB}}{L}\right)(t-t_6) & , \quad t_5 \le t \le t_6 \end{cases} \tag{7}$$

The mean square value of the output current ripple over one switching period is expressed in (8). This is expanded in (9) and (10).

$$\tilde{I}_{o1}^2 = \frac{1}{T_s}\int_{t_0}^{t_0+T_s} \tilde{\imath}_{o1}^2\, dt = \frac{2}{T_s}\int_{t_0}^{t_3} \tilde{\imath}_{o1}^2\, dt \tag{8}$$

$$\tilde{I}_{o1}^2 = \frac{2}{T_s}\left(\int_0^{T_0}\left(\frac{-\bar{v}_{AB}}{L}\right)^2 t^2\, dt + \int_0^{T_1}\left(\left(\frac{E_d-\bar{v}_{AB}}{L}\right)t + \left(\frac{-\bar{v}_{AB}}{L}\right)T_0\right)^2 dt + \int_0^{T_2}\left(\frac{-\bar{v}_{AB}}{L}\right)^2 t^2\, dt\right) \tag{9}$$

$$\tilde{I}_{o1}^2 = \frac{2}{T_s}\left(\begin{array}{c} \frac{1}{3}\left(\frac{-\bar{v}_{AB}}{L}\right)^2 T_0^3 + \\ \frac{1}{3}\left(\frac{E_d-\bar{v}_{AB}}{L}\right)^2 T_1^3 + \left(\frac{E_d-\bar{v}_{AB}}{L}\right)\left(\frac{-\bar{v}_{AB}}{L}\right)T_0 T_1^2 + \left(\frac{-\bar{v}_{AB}}{L}\right)^2 T_0^2 T_1 + \\ \frac{1}{3}\left(\frac{-\bar{v}_{AB}}{L}\right)^2 T_2^3 \end{array}\right) \tag{10}$$

The time intervals T_0, T_1 and T_2 in Figure 2(a) each is represented in (11)-(13) respectively.

$$T_0 = \frac{1-v_A^r}{4}T_s \tag{11}$$

$$T_1 = \frac{v_A^r-v_B^r}{4}T_s \tag{12}$$

$$T_2 = \frac{1+v_B^r}{4}T_s \tag{13}$$

From Figure 2(b), the current ripple in the interval of $\gamma \le \theta < \pi/2$ can be represented as (14).

$$\tilde{\imath}_{o2} = \frac{1}{L}\begin{cases} \left(-\frac{\bar{v}_{AB}}{L}\right)(t-t_0) & , \quad t_0 \le t \le t_1 \\ \left(\frac{E_d-\bar{v}_{AB}}{L}\right)(t-t_2) & , \quad t_1 \le t \le t_3 \\ \left(-\frac{\bar{v}_{AB}}{L}\right)(t-t_4) & , \quad t_3 \le t \le t_4 \end{cases} \tag{14}$$

The mean square value of the output current ripple over one switching period is in (15) and expanded in (16) and (17).

$$\tilde{I}_{o2}^2 = \frac{1}{T_s}\int_{t_0}^{t_0+T_s} \tilde{\imath}_{o2}^2\, dt = \frac{2}{T_s}\int_{t_0}^{t_2} \tilde{\imath}_{o2}^2\, dt \tag{15}$$

$$\tilde{I}_{o2}^2 = \frac{2}{T_s}\left(\int_0^{T_0}\left(\frac{-\bar{v}_{AB}}{L}\right)^2 t^2\, dt + \int_0^{T_1}\left(\frac{E_d-\bar{v}_{AB}}{L}\right)^2 t^2\, dt\right) \tag{16}$$

$$\tilde{I}_{o2}^2 = \frac{2}{T_s}\left(\frac{1}{3}\left(\frac{-\bar{v}_{AB}}{L}\right)^2 T_0^3 + \frac{1}{3}\left(\frac{E_d-\bar{v}_{AB}}{L}\right)^2 T_1^3\right) \tag{17}$$

The time intervals T_0 and T_1 in Figure 2(b) each is represented in (18) and (19) respectively.

$$T_0 = \frac{1-v_a^r}{4}T_s \tag{18}$$

$$T_1 = \frac{1+v_a^r}{4} T_s \tag{19}$$

Finally, the current ripple mean square over a fundamental period is expressed in (20).

$$\tilde{I}_{orms}^2 = \frac{2}{\pi}\int_0^{\gamma} \tilde{I}_{o1}^2 \, d\theta + \frac{2}{\pi}\int_{\gamma}^{\pi/2} \tilde{I}_{o2}^2 \, d\theta \tag{20}$$

The result is as (21).

$$\tilde{I}_{orms}^2 = \left(\frac{E_d}{Lf_s}\right)^2 \left(\frac{1}{96}\right) \begin{pmatrix} \left(\frac{3\sin(2\gamma)-6\gamma+4\pi}{\pi}\right) k^2 + \\ \left(\frac{6\cos(3\gamma)-54\cos(\gamma)-16}{3\pi}\right) k^3 + \\ \left(\frac{-3\sin(4\gamma)+24\sin(2\gamma)-36\gamma+24\pi}{8\pi}\right) k^4 \end{pmatrix} \tag{21}$$

Where $f_s = 1/T_s$ is the switching frequency.

3. EXPERIMENTAL SETUP

To verify the analytical result, experiments are carried out by using a capacitor start induction motor as the inverter load. The complete experimental setup is shown in Figure 3. The schematic diagram is shown in Figure 3(a) and the laboratory prototype is shown in Figure 3(b). Besides of the inverter and the induction motor, it consists of a transformer (number 1 in Figure 3(b)) to step down the voltage source from 220 V to 75 V and a three-phase rectifier with capacitor filter (number 2 in Figure 3(b)) to produce a DC voltage for the inverter. From this we get 183 Vdc power supply.

The inverter (number 3 in Figure 3(b)) is made of FGH40N60SFD 600V/40A IGBT and TLP350 optocoupler for the gate driver. The PWMs are programmed in TMS28379 digital signal processor. The switching frequencies are chosen to be not so high in order to get good precision in the ripple data. The inverter output current is sensed by using LA-55P LEM current sensor and recorded by a digital oscilloscope. Then, the recorded signal is passed to a high pass filter with a cut-off frequency of 450 Hz to get the current ripple signal. This is processed by PSIM software to produce the RMS (root mean square) of the current ripple.

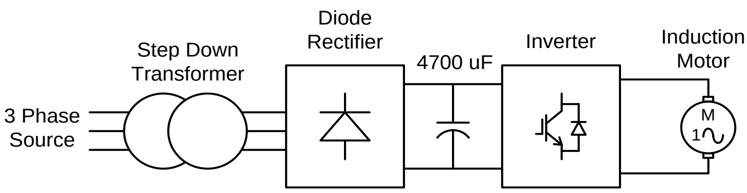

(a)

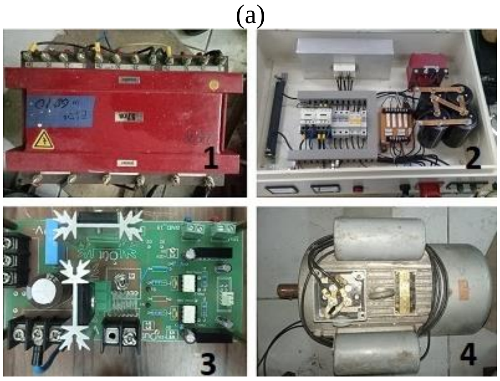

(b)

Figure 3. Experimental setup (a) schematic diagram and (b) laboratory prototype

The induction motor is shown in Figure 3(b) number 4. The capacitors are used during the starting time. During the running period, these capacitors are disconnected from the inverter (Figure 4(a)). The equivalent circuit of a single-phase induction motor when running is shown in Figure 4(b). The parameters in

Figure 4(b) are the stator resistance Rs of 3.18 Ohm, the stator leakage inductance Lls of 3.08 mH, the rotor resistance Rr of 2.63 Ohm, the rotor leakage inductance Llr of 3.08 mH, and the magnetizing inductance Lm of 54.31 mH. The inductance L in (21) is equal to the summation of the stator leakage inductance Lls and the rotor leakage inductance Llr. The experiments are conducted under no-load motor operation.

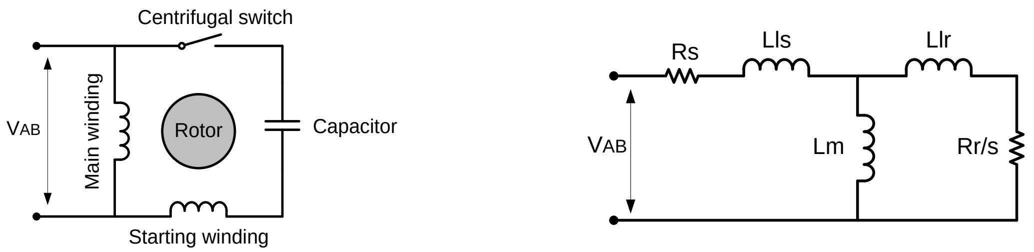

(a) (b)

Figure 4. Capacitor start induction motor: (a) circuit diagram and (b) equivalent circuit during running

4. RESULTS AND DISCUSSION

Based on (21), the graph of the normalized inverter output current ripples of SPWM and DPWMs for various discontinuous angle values is shown in Figure 5. In the figure, DPWMgamma means discontinuous PWM with a discontinuous angle of gamma. The DPWMs switching frequencies are normalized with respect to SPWM. From the graph, it can be seen that DPWM60 and DPWM75 give smaller current ripple than SPWM at high modulation index. DPWM60 produces a lower current ripple when the modulation index is more than 0.905. For DPWM75, the lower current ripple is obtained from a modulation index of more than 0.880. At a modulation index of 1.0, the DPWM60 can reduce the ripple by about 9.302% and DPWM75 reduce the ripple by about 6.312%. The DPWM45, DPWM30, and DPWM15 do not provide improvement. Because of this, it is DPWM60 and DPWM75 that will be clarified in the experiment. The DPWMs with discontinuous angles of 0º and 90º produce similar output current ripple to SPWM.

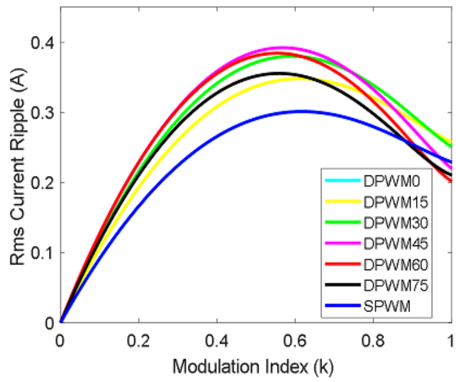

Figure 5. Inverter output current ripple as a function of modulation index

The experimental results are shown in Figure 6 and Figure 7, each with a modulation index of 1.0 and a modulation index of 0.5, respectively. The switching frequencies for SPWM, DPWM75, and DPWM60 are 2750 Hz, 3000 Hz, and 3300 Hz respectively. They are chosen for similar switching numbers in each modulation type during the fundamental period. From Figure 6, we can see that DPWM60 (Figure 6(a)) gives the smallest current ripple, followed by DPWM75 (Figure 6(b)) and SPWM (Figure 6(c)). From Figure 7, we can see clearly that DPWM60 (Figure 7(a)) produces the highest current ripple, and the lowest current ripple is provided by SPWM (Figure 7(c)). DPWM75 (Figure 7(b)) gives the middle current ripple. Those experimental results are matched with the predicted results in Figure 5. The current ripple RMS as a function of the modulation index is shown in Figure 8. The figure shows that the matching of the analytical and experimental results can be appreciated. The current ripples for modulation index greater than 0.3 only are considered here. This is because, for a modulation index less than 0.3, the motor can't start successfully.

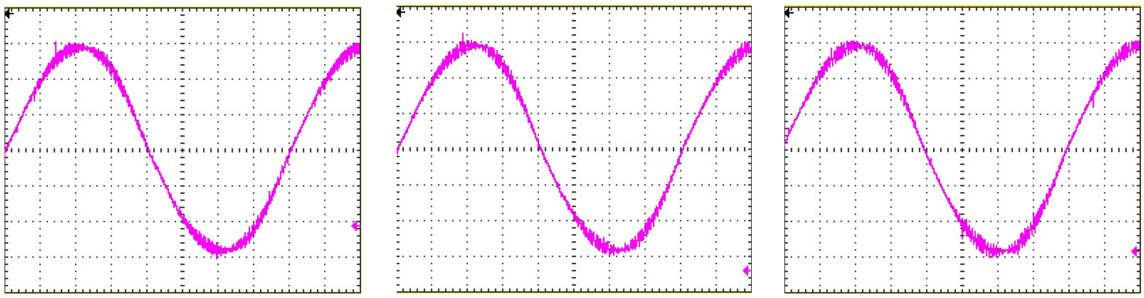

(a) (b) (c)

Figure 6. Inverter output current (3.33 Ampere/Div and 2.5 mS/Div) when the modulation index is 1.0: (a) DPWM60, (b) DPWM75, and (c) SPWM

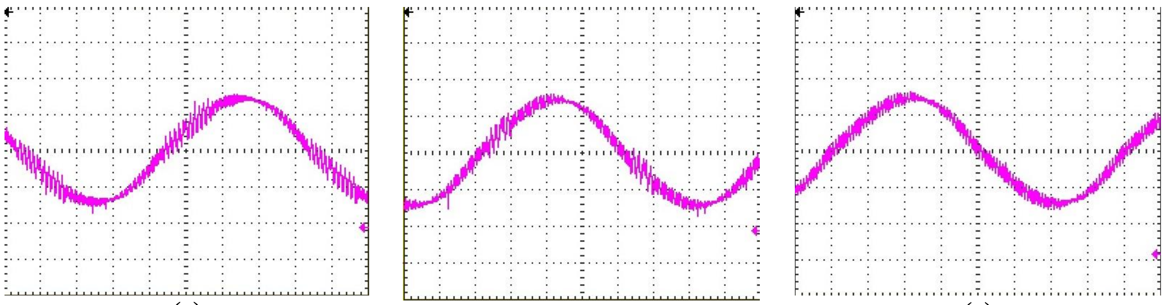

(a) (b) (c)

Figure 7. Inverter output current (3.33 Ampere/Div and 2.5 mS/Div) when the modulation index is 0.5: (a) DPWM60, (b) DPWM75 and (c) SPWM

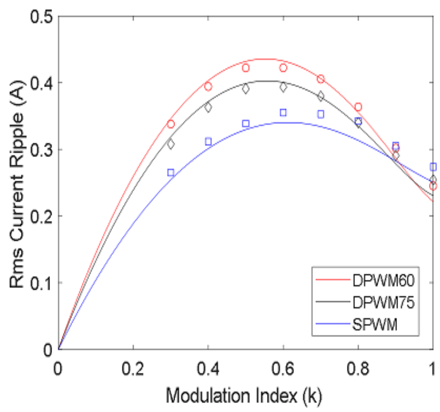

Figure 8. Inverter output current ripple as a function of modulation index

5. CONCLUSION

This paper proposes a DPWM for a single-phase full bridge inverter. The output current ripple has been calculated analytically and compared to the experimental results. The output current ripples resulting from DPWMs with discontinuous angles of 0º, 15º, 30º, 45º, 60º, 75º, and 90º have been presented. It is known that only DPWM60 and DPWM75 give benefits when compared to SPWM. The DPWMs produce a smaller current ripple compared to SPWM at a high modulation index (more than 0.880 for DPWM75 and 0.905 for DPWM60). The experimental results show agreement with the analytical calculation. In future research, variable switching frequency will be applied to the proposed modulation in the hope of producing a lower output current ripple.

REFERENCES

[1] A. S. Ba-thunya, R. Khopkar, K. Wei, and H. A. Toliyat, "Single phase induction motor drives - a literature survey," in *IEMDC*, 2001, pp. 911–916, doi: 10.1109/IEMDC.2001.939428.

[2] H. Deng, R. Oruganti, and D. Srinivasan, "Modeling and control of single-phase UPS inverters: a survey," in *IEEE PEDS*, 2005, pp. 848–853, doi: 10.1109/PEDS.2005.1619806.

[3] F. Chan and H. Calleja, "Reliability: a new approach in design of inverters for PV systems," *International Power Electronics Congress - CIEP*, pp. 97–102, 2006, doi: 10.1109/CIEP.2006.312159.

[4] W. Li, Y. Gu, H. Luo, W. Cui, X. He, and C. Xia, "Topology review and derivation methodology of single-phase transformerless photovoltaic inverters for leakage current suppression," *IEEE Transactions on Industrial Electronics*, vol. 62, no. 7, pp. 4537–4551, 2015, doi: 10.1109/TIE.2015.2399278.

[5] R. Musona and I. Serban, "Differential single-phase inverters with active power decoupling: a survey," *IEEE Access*, vol. 11, pp. 53654–53670, 2023, doi: 10.1109/ACCESS.2023.3280228.

[6] A. R. Gautam, D. M. Fulwani, R. R. Makineni, A. K. Rathore, and D. Singh, "Control strategies and power decoupling topologies to mitigate 2ω-ripple in single-phase inverters: a review and open challenges," *IEEE Access*, vol. 8, pp. 147533–147559, 2020, doi: 10.1109/ACCESS.2020.3015315.

[7] L. Hassaine and M. R. Bengourina, "Design and control technique for single phase bipolar H-bridge inverter connected to the grid," *International Journal of Electrical and Computer Engineering*, vol. 10, no. 3, pp. 3057–3065, 2020, doi: 10.11591/ijece.v10i3.pp3057-3065.

[8] A. S. Al-Khayyat, A. Al-Safi, and M. J. Hameed, "Single-phase grid-connected power control in dq synchronous reference frame with space vector modulation using FPGA," *Indonesian Journal of Electrical Engineering and Computer Science*, vol. 30, no. 1, pp. 57–69, 2023, doi: 10.11591/ijeecs.v30.i1.pp57-69.

[9] E. Radwan, M. Nour, A. Baniyounes, and K. S. Al-Olimat, "Design of type-1 servo controller for grid voltage modulated direct-power control of single-phase grid-connected PV inverter," *International Journal of Electrical and Computer Engineering*, vol. 11, no. 3, pp. 1912–1923, 2021, doi: 10.11591/ijece.v11i3.pp1912-1923.

[10] H. Attia, H. S. Che, T. K. S. Freddy, and A. Elkhateb, "Bipolar and unipolar schemes for confined band variable switching frequency PWM based inverter," *International Journal of Electrical and Computer Engineering*, vol. 11, no. 5, pp. 3763–3771, 2021, doi: 10.11591/ijece.v11i5.pp3763-3771.

[11] L. A. Mohammed, T. A. Husain, and A. M. T. Ibraheem, "Implementation of SHE-PWM technique for single-phase inverter based on Arduino," *International Journal of Electrical and Computer Engineering*, vol. 11, no. 4, pp. 2907–2915, 2021, doi: 10.11591/ijece.v11i4.pp2907-2915.

[12] P. Kiatsookkanatorn and N. Watjanatepin, "Novel ripple reduction method using three-level inverters with unipolar PWM," *Indonesian Journal of Electrical Engineering and Computer Science*, vol. 22, no. 3, pp. 1272–1283, 2021, doi: 10.11591/ijeecs.v22.i3.pp1272-1283.

[13] R. Shriwastava, S. Gosavi, S. S. Khule, S. Hadpe, and M. P. Thakare, "A novel PWM technique for reduced switch count multilevel inverter in renewable power applications," *International Journal of Applied Power Engineering*, vol. 12, no. 1, pp. 1–12, 2023, doi: 10.11591/ijape.v12.i1.pp1-12.

[14] M. Rasheed, M. M. A. Alakkad, R. Omar, M. Sulaiman, and W. A. Halim, "Enhance the accuracy of control algorithm for multilevel inverter based on artificial neural network," *Indonesian Journal of Electrical Engineering and Computer Science*, vol. 20, no. 3, pp. 1148–1158, 2020, doi: 10.11591/ijeecs.v20.i3.pp1148-1158.

[15] S. Chinnamuthu, V. Balan, K. Vaidyanathan, V. Chinnaiyan, and P. Santhanamari, "Analysis of single-phase cascaded H-bridge multilevel inverters under variable power conditions," *Indonesian Journal of Electrical Engineering and Computer Science*, vol. 30, no. 3, pp. 1381–1388, 2023, doi: 10.11591/ijeecs.v30.i3.pp1381-1388.

[16] P. A. Dahono, "New hysteresis current controller for single-phase full-bridge inverters," *IET Power Electronics*, vol. 2, no. 5, pp. 585–594, 2009, doi: 10.1049/iet-pel.2008.0143.

[17] J. W. Kolar, H. Ertl, and F. C. Zach, "Influence of the modulation method on the conduction and switching losses of a PWM converter system," *IEEE Transactions on Industry Applications*, vol. 27, no. 6, pp. 1063–1075, 1991, doi: 10.1109/28.108456.

[18] P. A. Dahono, Y. Sato, and T. Kataoka, "Analysis and minimization of ripple components of input current and voltage of PWM inverters," in *IEEE Transactions on Industry Applications*, vol. 32, no. 4, pp. 945–950, July/August 1996, doi: 10.1109/28.511653.

[19] J. A. Houldsworth and D. A. Grant, "The use of harmonic distortion to increase the output voltage of a three-phase PWM inverter," *IEEE Transactions on Industry Applications*, vol. IA-20, no. 5, pp. 1224–1228, 1984, doi: 10.1109/TIA.1984.4504587.

[20] P. A. Dahono, Deni, C. P. Akbarifutra, and A. Rizqiawan, "Input ripple analysis of five-phase pulse width modulated inverters," *IET Power Electronics*, vol. 3, no. 5, pp. 716–723, 2010, doi: 10.1049/iet-pel.2009.0129.

[21] A. Iqbal, E. Levi, M. Jones, and S. N. Vukosavic, "Generalised sinusoidal PWM with harmonic injection for multi-phase VSIs," *PESC Record - IEEE Annual Power Electronics Specialists Conference*, 2006, doi: 10.1109/PESC.2006.1712206.

[22] P. A. Dahono, "Analysis and minimization of output current ripple of multiphase PWM inverters," *in 37th IEEE Power Electronics Specialists Conference*, June 2006, pp. 1–6. doi: 10.1109/pesc.2006.1712231.

[23] D. Dujic, M. Jones, and E. Levi, "Analysis of output current ripple rms in multiphase drives using space vector approach," *IEEE Transactions on Power Electronics*, vol. 24, no. 8, pp. 1926–1938, 2009, doi: 10.1109/TPEL.2009.2017746.

[24] J. Prieto, M. Jones, F. Barrero, E. Levi, and S. Toral, "Comparative analysis of discontinuous and continuous PWM techniques in VSI-Fed five-phase induction motor," *IEEE Transactions on Industrial Electronics*, vol. 58, no. 12, pp. 5324–5335, 2011, doi: 10.1109/TIE.2011.2126540.

[25] L. Patnaik, G. Narayanan, and L. Umanand, "An investigation into even harmonic injection in pole voltages of a single-phase inverter," in *National Power Electronics Conference*, Roorkee, India, 2010, pp. 1–8.

[26] S. K. Asuri, "Modelling and control of sparse converter fed induction motor drives," Tennessee Tech Thesis, 2003.

[27] A. M. Mahfuz-Ur-Rahman, M. R. Islam, K. M. Muttaqi, and D. Sutanto, "An advance modulation technique for single-phase voltage source inverter to integrate SMES into low-voltage distribution," *IEEE Transactions on Applied Superconductivity*, vol. 29, no. 2, pp. 1–5, Mar. 2019, doi: 10.1109/TASC.2018.2882381.

[28] M. R. Chowdhury, S. Chowdhury, M. R. Islam, A. M. Mahfuz-Ur Razman, A. Z. Kouzani, and M. A. P. Mahmud, "An improved switching control technique for single-phase voltage source inverter," *IEEE International Conference on Applied Superconductivity and Electromagnetic Devices (ASEMD)*, 2020, pp. 1–2. doi: 10.1109/ASEMD49065.2020.9276322..

[29] L. Ferrer-Arnau, N. Berbel, G. J. Capella, and J. Zaragoza, "Study of modulation techniques applied to full bridge single-phase inverters based on wide-bandgap semiconductors," in *IECON 2019 - 45th Annual Conference of the IEEE Industrial Electronics Society*, Oct. 2019, pp. 2032–2037, doi: 10.1109/IECON.2019.8927267.

BIOGRAPHIES OF AUTHORS

Anwar Muqorobin studied electrical engineering at Universitas Diponegoro and Institut Teknologi Bandung. At present, he is a researcher at National Research and Innovation Agency (BRIN). His research activities are focused on inverter and control applications. He can be contacted at email: anwa014@brin.go.id.

Sulistyo Wijanarko received his bachelor's degree in Electrical Engineering from Universitas Gadjah Mada in 2013 and the master's degree from Institut Teknologi Bandung in 2021. At present, he is a research assistant at National Research and Innovation Agency, in Indonesia. His field of research is power electronics and drives. He can be contacted at email: sulistyo.wijanarko@brin.go.id.

Harjono Priyo Santosa received a bachelor's degree in Electrical Engineering from Jenderal Achmad Yani University (Unjani), Bandung, Indonesia in 2002. He is currently a researcher at the National Research and Innovation Agency (BRIN) and is interested in power converters. He can be contacted at email: harj001@brin.go.id.

Indrarini Dyah Irawati obtained B.E. and M.E. degree in Electrical Engineering at Telkom University, Bandung, Indonesia, and a doctoral degree from the School of Electrical and Information Engineering, Institute of Technology Bandung. She joined the School of Applied Science, Telkom University as an Instructor (2007-2013), worked as an assistant professor (2014-2018), associate professor (2019-2023), and professor (2023). Her main research interests are in the areas of compressive sensing, watermarking, signal processing, computer networks, and IoT. She can be contacted at email: indrarini@telkomuniversity.ac.id.